Understanding the cation-dependent surfactant adsorption on clay minerals in oil recovery

Liu, Zilong; Ghatkesar, Murali K.; Sudhölter, Ernst J.R.; Singh, Binder; Kumar, Naveen

DOI
10.1021/acs.energyfuels.9b03109

Publication date
2019

Document Version
Final published version

Published in
Energy and Fuels

Citation (APA)
Liu, Z., Ghatkesar, M. K., Sudhölter, E. J. R., Singh, B., & Kumar, N. (2019). Understanding the cation-dependent surfactant adsorption on clay minerals in oil recovery. *Energy and Fuels*, *33*(12), 12319-12329. https://doi.org/10.1021/acs.energyfuels.9b03109

energy&fuels
Article
Cite This: Energy Fuels 2019, 33, 12319−12329
pubs.acs.org/EF

Understanding the Cation-Dependent Surfactant Adsorption on Clay Minerals in Oil Recovery

Zilong Liu,*[†] Murali K. Ghatkesar,[‡] Ernst J. R. Sudhölter,*[†] Binder Singh,[†] and Naveen Kumar[†]

[†]Organic Materials & Interfaces, Department of Chemical Engineering, Faculty of Applied Sciences, Delft University of Technology, Van der Maasweg 9, 2629 HZ Delft, The Netherlands

[‡]Department of Precision and Microsystems Engineering, Faculty of Mechanical, Maritime and Materials Engineering, Delft University of Technology, Mekelweg 2, 2628 CD Delft, The Netherlands

Supporting Information

ABSTRACT: Surfactants have the ability to mobilize residual oil trapped in pore spaces of matrix rocks by lowering the oil−water interfacial tension, resulting in a higher oil recovery. However, the loss of surfactants by adsorption onto the rock surface has become a major concern that reduces the efficiency of the surfactant flooding process. In this study, the adsorption behavior of an anionic surfactant to a clay mineral surface was investigated by quartz crystal microbalance with dissipation monitoring upon variations with different cation conditions. Through recording the change of frequency and dissipation of clay-modified sensors, it allows us to do a real-time quantitative analysis of the surfactant adsorption with nanogram sensitivity. The results revealed that the surfactant adsorption increased in a Ca^{2+}-containing solution with increasing pH from 6 to 11, whereas from a Na^+-containing solution, more adsorption occurred at acidic conditions. The adsorbed amount went through a maximum (∼200 mM) as a function of the Ca^{2+} concentration, and the Voigt model suggested that multilayer adsorption of surfactants could be as many as 4−6 monolayers. Using mixed cation (Ca^{2+} and Na^+) solutions, the amount of adsorbed surfactant decreased linearly with decreasing fraction of $CaCl_2$, but Na^+ competed for about ∼30% adsorption sites. The importance of the presence of $CaCl_2$ for the surfactant adsorption was stressed in high-salinity and low-salinity solutions in the presence and absence of Ca^{2+}. Furthermore, increasing the temperature from 23 to 65 °C shows first a small increase of surfactant adsorption followed by a reduction of about 20%. The obtained results contribute to a better understanding of surfactant adsorption on clay surfaces and a guide to optimal flooding conditions with reduced surfactant loss.

1. INTRODUCTION

With their remarkable physicochemical properties of emulsification, foaming, detergency, dispersion, and solubilization,[1,2] surfactants have been widely used in numerous industrial processes such as water treatment,[3] mineral flotation,[4] and surfactant-based enhanced oil recovery (EOR).[5] In the application of EOR, batches of surfactant solutions are injected into the oil reservoirs for increasing the recovered oil yield. The addition of surfactants promotes the formation of microemulsions at the oil−water interface, thus significantly reducing the oil−water interfacial tension, and mobilizing the capillary-trapped oil or generating foam for a better sweep efficiency and alteration of the mineral wettability.[5−9] The main problem that affects the efficiency of oil recovery in the surfactant flooding process is the surfactant losses because of adsorption on reservoir rocks. High adsorption of surfactants causes chromatographic retardation when they are transported through reservoirs, rendering the chemical EOR processes less efficient and economically unfeasible.[10] To ensure effective propagation of surfactants in porous media, low adsorption is necessary and the adsorption dynamics must be well understood.

In the surfactant−water−solid system, the quantity of surfactant adsorption depends on the solid chemistry (i.e., rock composition and surface charge), surfactant characteristics, water composition (i.e., salinity, ions, pH), and the system temperature.[7,8,11−15] The rock surface can be either positively or negatively charged by ionization/dissociation of surface groups in the aqueous medium or by the adsorption of ions from solution. For example, silica surfaces are predominantly negatively charged, whereas calcite and dolomite are positively charged at neutral pH.[16,17] If the injected surfactants and the reservoir rock have opposite charges, the adsorption process is favored, and thus equilibration time is fast. Conversely, if they have the same charge, repulsive interaction will result in negligible adsorption.[18] The addition of alkali to raise the solution pH is able to change the mineral charge sites,[19] and thus alter the adsorbed amounts of surfactants. Solairaj et al.[20] found that the retention of anionic surfactants to silica rock decreased from 0.22 to 0.08 mg/g when the pH was increased from 6 to 11. This observation was consistent with the results from Tagavifar et al.,[7] who concluded that the adsorption of anionic surfactants decreases approximately linearly with pH of above 9.

Another essential factor affecting the loss of anionic surfactants to the reservoirs is the salinity of the solutions. Increasing the salinity can increase the adsorption of surfactants on the rock surface because of the resulting decrease in the Debye screening length, thus reducing the electrostatic repulsion between the adsorbed molecules and

Received: September 11, 2019
Revised: November 1, 2019
Published: November 14, 2019

DOI: 10.1021/acs.energyfuels.9b03109

rock surfaces.[21,22] Moreover, the salinity also changes the surface charges for the adsorption. AlQuraishi et al.[23] observed a substantial increase in the magnitude of the negative surface charges of sandstone rock when switching from high-salinity (HS) seawater to diluted low-salinity (LS) seawater. Therefore, the anionic surfactant adsorption would decrease in LS solutions as the number of negatively charged sites increases.[24] The presence of divalent cations such as Ca^{2+} can cause a significant increase in the adsorption of anionic surfactants to negatively charged surfaces, but contrary for cationic surfactants to a considerable decrease in adsorption.[8,25,26] The reported adsorption isotherms confirmed this by showing twice the amount of adsorption of sodium dodecyl sulfate by the addition of Ca^{2+} compared to Na^+.[27] Nonetheless, the influence of temperature affects the surfactant adsorption depending upon several factors, including brine compositions, salinity, and the investigated rocks.[14]

Based on the composition of the rocks, oil reservoirs are generally divided into sandstone and carbonate, with the presence of clay minerals. For sandstones, anionic surfactant adsorption primarily depends more on the presence of the amount of clay than quartz or silica.[20,28] In the understanding of LS water flooding, the presence of both clay minerals and divalent cations were necessary, in particular for the surface reactions.[29,30] Because of the high clay content of carbonate reservoirs, significant adsorption of surfactant and polymer was found.[31] Ma et al. observed a negligible adsorption of a cationic surfactant on synthetic calcite (no clay was present), whereas the adsorbed amount was substantial on natural limestone and could be positively correlated with the clay content as deduced from the observed aluminum and silicon content of the rock.[32] In this picture, clay minerals, such as kaolinite, smectite, illite, and chlorite, on the rock surfaces have been claimed as key in the performance of the surfactant adsorption. It was found that the clay structure and surfactant nature had a significant influence on the adsorption capacity of surfactants.[33,34] Torn et al.[35] reported the mixed adsorption of the nonionic polymer and the anionic surfactant on kaolinite controlled by the surface charge. Rodríguez-Cruz et al.[36] suggested that the main parameter affecting the adsorption of sodium dodecyl sulfate was the presence of organic matter and kaolinite in the soil. Surfactant adsorption isotherms had been performed to derive the information about the interaction mechanism between anionic surfactants and clay.[37] The calcium−surfactant complexes played a role in the adsorption on kaolinite[38] and the adsorption mechanism of hexanoate on the clay model surface was proposed by the presence of Ca^{2+}.[39] However, there is no systematic and quantitative understanding of how and to what extent cations affect the adsorption processes and the dependence on temperature.

To address the abovementioned issues, we aim to understand the cation (Ca^{2+} and Na^+)-dependent adsorption of an anionic alcohol alkoxy sulfate (AAS) surfactant on clay mineral surfaces using quartz crystal microbalance with dissipation monitoring (QCM-D). Through recording the changes in frequency (because of mass adsorption) and dissipation (because of viscoelasticity), QCM-D measurements allow for a quantitative investigation of the surfactant adsorption behavior. In this work, a fundamental study was conducted to explore the effect of the monovalent Na^+ and divalent Ca^{2+} on the AAS adsorption behavior on clay surfaces. The purpose of our study was (i) to compare the results from two types of salt solutions as a function of pH, electrolyte concentrations, and temperature, (ii) to gain insights into the processes that control adsorption behavior under the conditions of both mixed cation (Na^+ and Ca^{2+}) solutions and HS/LS solutions, (iii) to understand the adsorption mechanism of surfactants to clay surfaces, and (iv) to conclude with the implications for reducing surfactant adsorption in EOR based on the obtained new understanding.

2. EXPERIMENTAL METHODS

2.1. Chemicals and Solutions. The anionic surfactant (AAS-J771, hereafter abbreviated as AAS, had a molecular weight of 700 g/mol) was supplied by the Shell Oil Company. Such a surfactant typically contains mainly C_{12} and C_{13} alkyl-groups and seven propoxy groups in the middle part connected to the sulfate head group. It is a negatively charged surfactant commonly used in EOR with the advantages of excellent divalent cation tolerance (no precipitation in the presence of relatively high Ca^{2+} concentrations) and a relatively low cost compared to other types of EOR surfactants.[40] The AAS surfactant was used as received without any further purification. All salt solutions were prepared by mixing the deionized water (Milli-Q, with a resistivity of >18.2 MΩ·cm) with reagent-grade salts (NaCl and $CaCl_2$), which were purchased from Sigma-Aldrich and had a purity grade of >97.0%. The salt solutions were mixed with surfactants at a concentration of 0.15 wt % (2.1 mM), which was well above the critical micelle concentration of ∼0.04 mM as measured at room temperature and in the absence of added salts. The prepared surfactant solutions were shaken with a vortex shaker (Scientific Industries, Vortex-Genie 2, the intensity of 5) for 30 min to obtain well-dispersed and stable solutions. The solution pH was adjusted using 0.2 M HCl and 0.2 M NaOH and monitored using a Metrohm 827 pH meter.

2.2. Clay Sensors. Standard clay sensors (QSX 999, Q-sense) were purchased from Q-Sense Biolin Scientific. The gold-coated quartz crystal sensor was coated with a thin layer of Boise rock. This is a type of smectite rich clay with mixed layers of illite-smectite, containing small amounts of chlorite and kaolinite. Smectite belongs to the class of aluminum phyllosilicates. Generally, the surface charge of clay minerals at neutral pH is negative[41] because of the presence of dissociated surface hydroxyl groups. The sensors consist of an AT-cut quartz crystal disk (14 mm in diameter) with metal electrodes deposited on both sides. One side was covered with a thin clay layer (∼100 nm in thickness) with 50 nm SiO_2, 100 nm Au, 50 nm Ti, and 5 nm Cr sputter-coated onto the crystal surface. The fundamental resonance frequency (f_0) for the clay-modified sensor crystals was 5 MHz. Prior to each experiment, the sensors were rinsed successively with Milli-Q, ethanol, and iso-propanol three times to remove any possible surface contaminations coming from the air. It was then gently dried by a stream of clean and dry nitrogen gas. The dried sensors were finally plasma-cleaned at 1000 mTorr (Harrick Plasma Cleaner, 110 V, medium intensity) for 5 min. After plasma-cleaning, the sensors were immediately transferred into flow modules and properly aligned to the desired position. The possible reuse of the sensor depends on the reproducibility of the signal during measurements. To minimize signal drift, each sensor was only used less than five times before obvious variation of signals occurred, such as an unstable reference signal.

2.3. Surface Characterizations. Atomic force microscopy (AFM) tomography images were acquired in tapping mode using a silicon tip (NSG03, NT-MDT), with a nominal value of the tip radius of 7 nm and a nominal spring constant of 0.4−2.7 N/m. Images were recorded over a 2 × 2 μm^2 area with 512 × 512 data points, at room temperature, and at a scan rate of 1 Hz. The morphology of the sensor surfaces at a larger area were studied by scanning electron microscopy (SEM) using a JSM-6010LA InTouchScope. The SEM was operated under high voltage and vacuum mode at magnifications of 200−10 000 times. The chemical state and the element composition of the clay sensors were determined with X-ray photoelectron spectroscopy (XPS) spectra (K-Alpha Thermo Fisher Scientific spectrometer), using monochromatic Al Kα radiation at room temperature. To calibrate the obtained XPS spectra, the main peak of carbon (C 1s) was adjusted to the reference value of ~284.8 eV.[42,43] Sputtering was carried out by an argon ion gun. During the sputtering, the chamber pressure was ~4 × 10^{-7} Torr and the ion gun was operated at 1 kV and 1 mA.

2.4. QCM-D Principles. QCM-D has been widely used to investigate the adsorption and desorption processes of molecules on solid surfaces with nanogram sensitivity.[16,26] In this work, a QCM-D (E1, Q-sense) and its high temperature module were used to investigate the adsorption behavior of surfactants to the clay-modified sensor surface. The QCM-D simultaneously measures the changes in resonant frequency and dissipation energy of the clay-modified coated crystals. By application of an alternating voltage across the electrodes, shear stress is generated because of the piezoelectric property of quartz and this results in oscillation of the crystal at its resonance frequency (f). Any increase in adsorbed mass (Δm) because of a binding process to the surface causes a shift in the resonance frequency to lower values (Δf). The linear relationship between Δm and Δf can be described by the Sauerbrey equation[44]

$$\Delta f = -\frac{2nf_0^{\,2}\Delta m}{\rho_q v_q} = -\frac{n\Delta m}{C} \tag{1}$$

where C is the sensitivity constant of the quartz crystal (0.177 mg m^{-2} Hz^{-1}), n is the overtone number (1, 3, 5, etc.), ρ_q is the specific density of quartz (2650 kg/m^3), and v_q is the shear wave velocity in quartz (3340 m/s). The Sauerbrey equation is valid when the adsorbed film is thin, rigid, homogeneously distributed, and does not slip at the clay–water interface. This may not be always the case, especially when the adsorbed film shows viscoelastic properties and does not fully couple to the substrate. Under such conditions, the Sauerbrey equation would underestimate the amount of adsorbed mass.

The decoupling of adsorbed molecules leads to a damping of the oscillation and the energy dissipation of the sensor (ΔD) was measured to estimate the viscosity and elasticity of the adsorbed layer.[45]

$$\Delta D = -\frac{E_D}{2\pi \Delta E_S} \tag{2}$$

where E_D is the energy dissipated during one oscillation period and E_S is the total energy stored in the oscillation system. ΔD presents the viscoelastic changes of the adsorbed layer and a large change of ΔD indicates a soft or loosely bound layer to the surface, whereas small changes are indicative of a flat and rigid adsorbed layer. The measurement of ΔD allows a more accurate estimation of the adsorbed mass in a viscous film by introducing the viscosity and shear elastic modulus as described in the Voigt model,[46] which is implemented in the Dfind software from Q-sense. The Voigt model is usually applied to adsorbed polymers, which conserve their shape under shear deformations and do not flow.[46] In the fitting using the Voigt model, the parameter chi-square (χ^2) is used to describe the fit quality.

$$\chi^2 = \sum_i [(Y_{\text{theory},i} - Y_{\text{mea},i})/\sigma_i]^2 \tag{3}$$

where the sum is taken over all measured points and σ_i is the standard deviation of the ith data point. The model function Y_{theory} is the theoretical shift in resonant frequency that is related to the four physical parameters of the adsorbed film: film thickness, density, shear modulus, and viscosity and Y_{mea} is the set of measured values. The lower the χ^2, the better the fitting to the model. If the density is known, the thickness, viscosity, and elasticity of the adsorbed layer can be calculated. It is recommended that the number of selected overtones has to be larger than the number of fitted parameters. Therefore, for the fitting of thickness, viscosity, and shear modulus, at least three overtones need to be selected. For our system, the density of bulk fluid and adsorbed layer are both set at 1000 g/L. Recently, Radke et al.[47] built a viscosity–density correction to Δf based on the simplified Voigt model of a thin adsorbed film.

$$\frac{\Delta f}{n} = -\frac{\Delta m}{C} - \frac{\Delta D f_0}{2} \tag{4}$$

When solute adsorption is strong from a dilute solution, such a correction is not important.[47] In this study, the mass variations have been calculated and estimated with the above models and corrections.

2.5. QCM-D Experimental Procedures. The QCM-D flow modules and connecting tubes were cleaned before each experiment, by following a similar procedure as used for the clay sensors but now without plasma treatment. Figure 1 illustrates the subsequent steps involved in the adsorption investigation of surfactant to clay surfaces. The Milli-Q water was initially flushed through the flow modules with a peristaltic pump (ISMATEC, ISM935C) at a flow rate of 200 μL/min. The resonant frequency and dissipation of various overtones were recorded simultaneously. The fifth harmonic of the fundamental resonance frequency showed a good signal-to-noise ratio and was therefore chosen for our work. After obtaining a stable reference signal, the clay surface was flushed with a salt solution in step 2, which produced a negative frequency shift because of the larger density and viscosity of the salt solution compared to Milli-Q water only. In step 3, it was followed by a continuous injection of the surfactant solution. The further change of frequency shift depends on the surfactant adsorption. The solution was changed back to Milli-Q or salt solutions to desorb the adsorbed surfactants and to evaluate the desorption processes. The measurements were repeated 2–4 times for each kind of salt and surfactant solution to ensure the accuracy and reproducibility of the data. After each experiment, the entire system was flushed with Milli-Q at 200 μL/min for 45 min. All experiments were performed at room temperature (23 ± 0.1 °C) and pH = 9, except for the investigation of the pH and temperature effects. The averaged values for the QCM-D data are given and have been used for the calculations presented in this research.

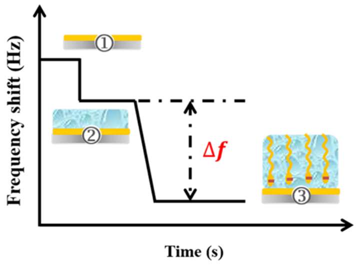

Figure 1. Schematic representation of the applied QCM-D measurement procedures for the investigation of AAS surfactant adsorption to clay mineral surfaces. ① A bare clay-modified sensor in Milli-Q water, ② in the added salt solution, ③ then followed by a continuous injection of the surfactant solution. The frequency shift Δf indicates the surfactant adsorption to the surface.

3. RESULTS AND DISCUSSIONS

3.1. Surface Characterizations. The AFM and SEM images of the clay-modified quartz crystals applied in QCM-D are shown in Figure 2. The surface was dominated by very small clay nanoparticles with a size of ~50 nm that were evenly distributed (see Figure 2a). Such clay nanoparticles were also observed on the surface of the quartz crystals in sandstones and on calcite particles in chalk.[48] The average surface roughness and root mean square deviation in the height of clay-modified quartz crystals were 1.85 and 2.37 nm, respectively. In the SEM image shown in Figure 2b, no characteristic topography was found on the larger area surface (except for a few pieces of dust, as shown on the right of the SEM image) on the received sensor without any treatment.

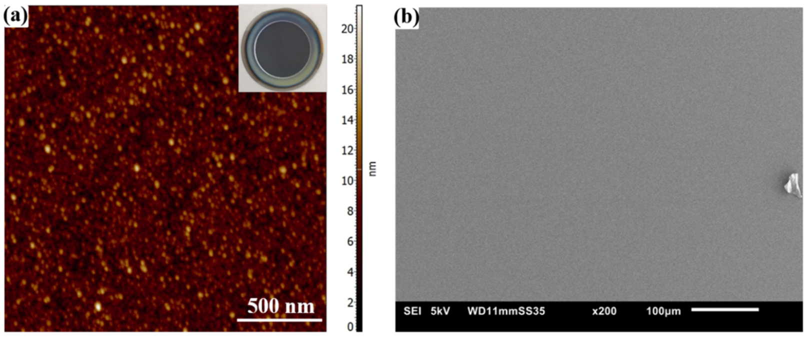

Figure 2. (a) AFM topography image (2×2 μm^2) of the clay-modified surface. The inset is the complete clay-modified sensor used for QCM-D measurements. (b) SEM image of larger surface area, 200 times magnified.

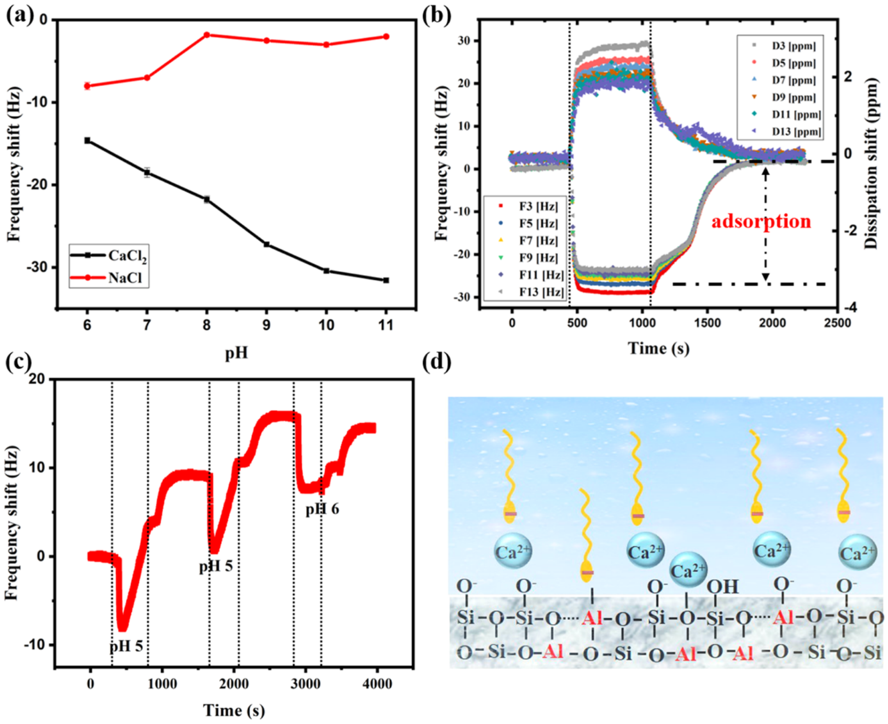

Figure 3. (a) Effect of pH on the surfactant adsorption to the clay surface in 100 mM NaCl and 100 mM $CaCl_2$ solutions. (b) Real-time observed frequency and dissipation shifts for the different overtones of a QCM-D resonator upon surfactant adsorption in 100 mM $CaCl_2$ solutions, at pH 9. (c) Real-time experimental data of frequency shifts in 100 mM NaCl solution, at pH 5 and 6. (d) Schematic illustration of the adsorption mechanism at the water−clay interface. The dashed lines indicate fluid switching between salt solutions and surfactant solutions.

The high-magnification SEM images of the same area can be found in Figure S1. These surfaces were considered to be sufficiently flat and smooth. Therefore, the possible influence of frequency shift from the liquid trapping effect because of surface roughness was neglected. Any differences in adsorption behavior were attributed to water composition and surfactants. The chemical state and the elemental composition of the clay-modified surface after sputtering are shown in Figure S2 and Table S1. Through XPS analysis, relative percentages of oxygen, silicon, and alumina were 43.5, 28.3, and 19.9 at. %, respectively. The clay mineral was mainly composed of aluminum hydroxide and silicate.[43] Copper (Cu^{2+}) ions were also determined and minor amount ions of Ca^{2+}, Mg^{2+}, K^+, and Na^+ were seen as the exchangeable cations. The surface hydroxyl groups or oxygen were the main negative surface sites of the clay,[49] where adsorption might occur.

3.2. pH Effect.

The adsorption of AAS to the clay surface was monitored starting from an aqueous AAS solution [0.15 wt % corresponds to 2.1 mM, which was well above its critical micellar concentration (cmc)] at room temperature (23 ± 0.1 °C). The solution was applied via a flow system, as described in Section 2.5, to the QCM-D sensor. The observed frequency shift is plotted as a function of pH for both 100 mM NaCl and 100 mM $CaCl_2$ containing solutions in Figure 3a. A larger frequency reduction indicates a larger amount of adsorbed mass to the clay-modified sensor surface. In the presence of Ca^{2+} ions, the AAS adsorption increased with increasing pH, whereas in the presence of Na^+ ions, the opposite was seen: AAS adsorption decreased with increasing pH. Above pH = 8, hardly any effect was observed for Na^+, indicating negligible AAS adsorption. From these results, it was clear that the presence of Ca^{2+} ions enhanced the AAS adsorption to the clay surface. This effect was more pronounced at higher pH, where dissociation of surface hydroxyl groups was more prominent, leading to more surface sites for binding.[35]

DOI: 10.1021/acs.energyfuels.9b03109
Energy Fuels 2019, 33, 12319−12329

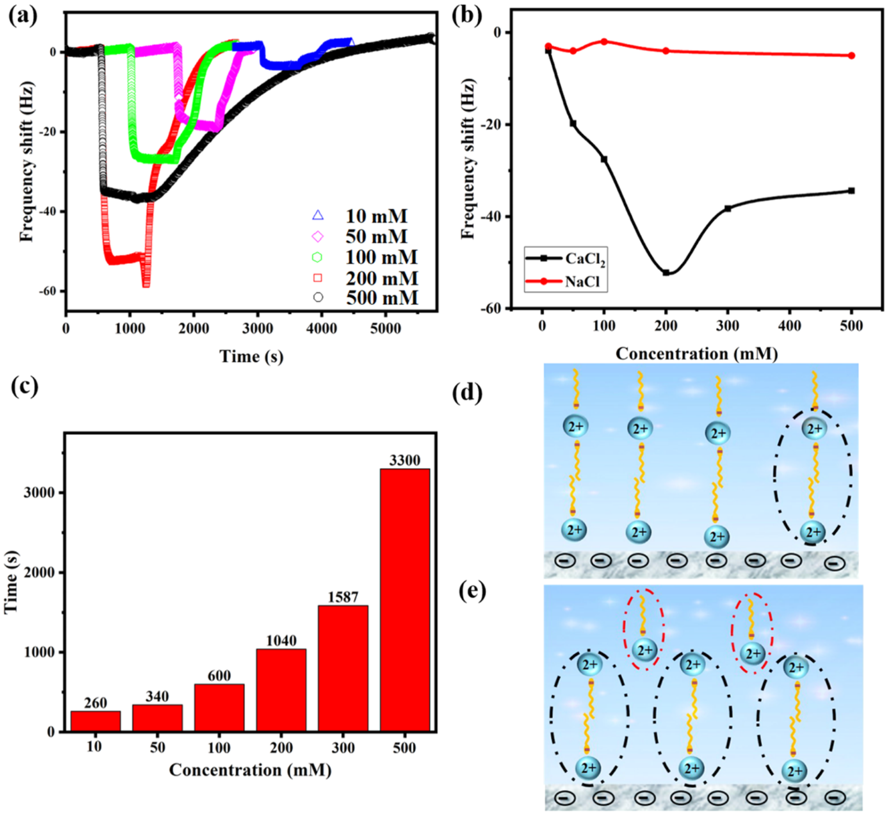

Figure 4. (a) Real-time observed frequency shifts of a clay-modified QCM-D sensor upon addition of AAS (0.15 wt %) and subsequent flush without AAS at pH = 9 and room temperature with varying $CaCl_2$ concentrations. For clarity, the start of the curves were offset. (b) Observed maximum frequency shifts as a function of NaCl and $CaCl_2$ concentration. (c) Desorption time of AAS surfactant as a function of the applied $CaCl_2$ concentrations. (d) Schematic illustration of the adsorbed AAS surfactants to the clay surface via Ca^{2+} bridging for the multilayer adsorption, such as the double layer film in the black circle. (e) Screening effect of Ca^{2+} leads to the formation of positively charged $Ca(RSO_4)^+$ complexes (red dash circle).

A typical example of frequency and dissipation changes for different overtones with time is shown in Figure 3b for the situation of 100 mM $CaCl_2$ and pH = 9. For different overtones, the observed shifts were similar. The observed frequency shifts were negative because of the increase of adsorbed mass, whereas the positive dissipation shifts indicated a soft, possible loosely bound layer on the clay surface with energy dissipated. From the sharp decrease in frequency shift, it was concluded that the adsorption was fast. Desorption was found to be slower, which was in agreement with the positive affinity of AAS surfactants to the clay surface. The desorption was interpreted as a two-step process: an initial release of weakly bound surfactants and later a process related to the desorption of strongly bound surfactants.

At pH = 5 in the presence of 100 mM NaCl (Figure 3c), injection of AAS, followed by the same salt solution, showed a rapid negative frequency shift (increase in adsorbed mass), followed by a positive frequency shift (desorption of mass), ending at a final mass lower than the initial value. This was observed again upon repeating the experiment. At pH = 6, overall an effective increase in crystal mass was observed. The overall mass decrease points to the possible etching of the clay and thus instability of the clay-modified sensor at pH = 5, and therefore we have set out pH values always ≥6 in all our subsequent experiments.

It is proposed that the sulfate anionic head group of AAS binds to the negatively charged clay surface via a bridging Ca^{2+} ion (Figure 3d). A prerequisite for such an interaction is a negative surface charge. Such a charge is determined by the pH of the solution. For silica surfaces, the isoelectric point is at pH = 2 and the surface will be negatively charged above that pH.[16] At our conditions of pH ≥ 6, the silica surface is negatively charged because of the dissociation of surface silanol (−SiOH) groups. The clay mineral surfaces not only contain −SiOH groups but also −AlOH sites on the octahedral aluminous sheet. The −AlOH has a higher pK_a compared to −SiOH; the isoelectric point of clay is therefore higher than silica,[50−52] indicating that the negative charge density of clay is less than that of silica at a given pH. The charge on the clay surface could be the result of either the hydrolysis of −SiOH or Lewis acid−base interactions in −AlOH or because of adsorption of the cation−surfactant complexes. At a lower pH region, with reduced negative surface charge, parts of the clay surface could be still positively charged in NaCl solution, where electrostatic forces play a role in the adsorption of the anionic surfactant. Moreover, the ligand exchange could not be ruled out and the sulfate groups may exchange with hydroxyl groups in Al(III) sites, and the AAS surfactants directly attach to positively charged sites at the clay surfaces. This observation is consistent with higher sodium dodecyl sulfate adsorption on the sand surface at acidic conditions.[53] When pH is above 8, it carries a negative surface charge because of deprotonation of −SiOH groups and the hydroxide ions compete for the adsorption sites of Al(III). Therefore, anionic surfactants have a lower adsorption value in NaCl solution because of the fewer Al(III) sites, compared to negative charges with Ca^{2+}.

DOI: 10.1021/acs.energyfuels.9b03109
Energy Fuels 2019, 33, 12319−12329

Table 1. Results of Interpretation of the QCM-D Data of Different Overtones for AAS (0.15 wt %) Adsorption in the Presence of 100 mM $CaCl_2$ Solution at pH = 9 and Room Temperature

	Sauerbrey			Voigt[a]	simplified Voigt		
	F_3[b]	F_5	F_7	averaged	F_3	F_5	F_7
mass (ng/cm^2)	529 ± 2	492 ± 2	468 ± 2	1250 ± 30	390 ± 2	369 ± 2	353 ± 2
thickness (nm)	4.8 ± 0.01	4.5 ± 0.02	4.3 ± 0.02	11.3 ± 0.3	3.5 ± 0.01	3.4 ± 0.01	3.2 ± 0.02

[a] Averaged adsorbed amount for all overtones (1, 3, 5, ..., 13). [b] F_n is the resonant frequency shift of the *n*th overtone.

Table 2. Results of Interpretation of AAS (0.15 wt %) Adsorption in the Presence of Varying $CaCl_2$ Concentrations at pH = 9 and Room Temperature Using the Voigt Model

$CaCl_2$ concentration (mM)	10	50	100	200	300	500
mass (ng/cm^2)	319 ± 9	1040 ± 35	1250 ± 30	2600 ± 14	1720 ± 54	1240 ± 39
thickness (nm)	3.2 ± 0.1	10.4 ± 0.4	11.3 ± 0.3	26.0 ± 0.1	17.1 ± 0.5	12.4 ± 0.4
chi-square (χ^2)	0.005	0.01	0.01	0.18	0.01	0.5

In a previous study on LS effect, it also proposed the Ca^{2+} bridging between negatively charged organic molecules and the surface, but no bridging occurred for Na^+.[21,54] In the absence of Ca^{2+} ions and the presence of the monovalent Na^+ ions, this bridging is not possible and therefore no AAS adsorption is observed. The finding of higher adsorption from Ca^{2+} solutions and negligible adsorption in Na^+ solutions at higher pH is therefore consistent with the proposed cation bridging mechanism. As surfactant flooding is always accompanied with alkalis to raise the solution pH, the following studies were performed at alkaline conditions of pH 9.

3.3. Salt Concentration. The AAS surfactant adsorption and desorption was next studied under the same conditions as before, but now at pH = 9 and with varying aqueous salt concentrations (10−500 mM of $CaCl_2$ and NaCl) and the results are shown in Figure 4. In Figure 4a, the frequency shift is plotted in real time for different applied $CaCl_2$ concentrations. For clarity, the start of each response was shifted in this figure. For every investigated condition, a fast decrease of frequency was observed with an adsorption time of 50−200 s, indicating that adsorption is always a fast process. A higher concentration of $CaCl_2$ shows a larger frequency shift, which is interpreted by more AAS adsorption. A maximum of adsorption is observed at 200 mM (Figure 4b). Increasing the $CaCl_2$ concentration to 500 mM shows a decrease of frequency shift, indicating the loss of adsorbed AAS. Replacing the $CaCl_2$ by NaCl of the same concentrations shows hardly any change of frequency shift, thus no AAS adsorption. This observation stresses the importance of the presence of $CaCl_2$ for the adsorption of AAS to the clay surface.

By switching the flow solution from AAS-containing to the absence of AAS, we were able to monitor a decrease of frequency shift in time for the applied $CaCl_2$ concentrations. The time needed to displace the adsorbed AAS from 5 to 95% is presented in Figure 4c for the different $CaCl_2$ concentrations. For increasing $CaCl_2$ concentrations, the AAS desorption time becomes increasingly longer; thus, the higher the $CaCl_2$ concentration, the slower the process. This indicates a two-step desorption process for the higher $CaCl_2$ solutions. To interpret the above observation, the observed frequency shifts and dissipation shifts were analyzed according to the Sauerbrey and Voigt models in the next section.

3.4. Adsorption Calculations and Modeling. We have analyzed the experimental data of frequency shift and dissipation shift for the clay-modified sensors with QCM-D for the adsorption of AAS (0.15 wt %) in the presence of 100 mM $CaCl_2$ at pH = 9 and at room temperature. From the different overtones, the mass and thickness of the adsorbed AAS layer have been calculated. See Section 2.4 for more details. The results are presented in Table 1. It can be seen that the adsorbed amount and layer thickness calculated using the Sauerbrey equation and the simplified Voigt model are overtone-dependent, which is consistent with previous results.[47,55] Both calculated mass and thickness are lower with increasing overtone number. As for the Voigt model, all the overtones (1 to 13th) were applied to derive the adsorbed mass and layer thickness. The chi-square (χ^2) is about 0.01, indicating a perfect fit with the Voigt model. What can be expected for the adsorption of a single AAS monolayer? Assuming that a tightly packed monolayer occupies 20−30 Å^2/molecule,[56,57] and using for AAS a molecular weight of 700 g/mol, such a monolayer would result in a mass increase of 389−583 ng/cm^2. This value range matches very nicely with the interpretation using the Sauerbrey and simplified Voigt models. However, because of our observed significant dissipation shifts and separations such as in Figure 3b, it is expected that the monolayer(s) formed are not rigid as assumed in these two models. The Voigt model seems therefore more appropriate. Thus, a less dense and less rigid multilayer of ∼11 nm thickness seems more likely. Using a value of 3−4 nm for the length of a single AAS molecule suggests that there is room for the adsorption of 3−4 AAS layers. It is important to realize that surfactants adsorbed to surfaces and in contact with an aqueous solution and preferentially having the outer layer exposed to the aqueous phase have a hydrophilic character; thus, it is more likely that the anionic head group points outward, and not the hydrophobic tail.

We continue now using the Voigt model for the interpretation of the frequency shift and dissipation shift for the clay-modified sensors in QCM-D for the adsorption of AAS (0.15 wt %) in the presence of increasing $CaCl_2$ concentrations at pH = 9 and at room temperature. From the averaged overtones (1 to 13th) the mass change and thickness change of the adsorbed AAS layer have been calculated. See Section 2.4 for more details. The results are presented in Table 2. The calculated mass increase grows up to a $CaCl_2$ concentration of 200 mM, as does the thickness increase. The maximum adsorption layer is 4−6 (2 or 3 stacked bilayers) in 200 mM $CaCl_2$ solution. This multilayer adsorption has also been observed on mica surfaces, with as many as six layers through three stacked bilayers.[58] It should be pointed out that under these high $CaCl_2$ concentrations with

DOI: 10.1021/acs.energyfuels.9b03109
Energy Fuels 2019, 33, 12319−12329

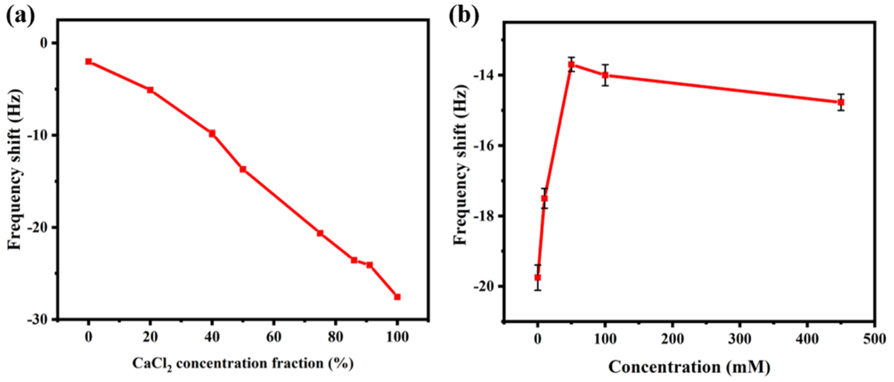

Figure 5. (a) Effect of $CaCl_2$ concentration fraction on the frequency shift in mixed $CaCl_2$ + NaCl solutions of totally 100 mM. (b) Effect of increasing Na^+ concentrations on the frequency shift at constant 50 mM Ca^{2+}.

the 0.15 wt % of AAS, these solutions are still stable during measurements. Precipitation of calcium AAS, and therefore a reduction of cmc (less AAS monomers available for adsorption) can be excluded, as these mixtures have been tested in a separate experiment and observed to be stable and well-dispersed solutions. Therefore, the adsorbed mass and thickness decrease by increasing the $CaCl_2$ concentration from 200 to 500 mM needs to be explained by the stability of the adsorbed layer. It is speculated that the growing layers are initially of low density and low rigidity. Upon growing, they might collapse to thinner and more rigid multilayers. The suggestion of more rigid multilayers at high $CaCl_2$ concentrations is supported by our observation that the desorption rate under these conditions is lower compared to the conditions of low $CaCl_2$ concentrations (see Section 3.3). The increased stability of the adsorbed layer at a higher $CaCl_2$ concentration form 200 to 500 mM could come from two aspects: (1) the increased electric double layer force is dominant compared to the cation bridging, which favors strong adsorption and thus needs a longer time for the desorption. (2) The strong screening effect of Ca^{2+} leads to the formation of positively charged $Ca(RSO_4)^+$ complexes (R is the rest of surfactant), as shown in the blue dashed circle of Figure 4e. The multilayer adsorption through cation-bridging was collapsed because of the electrostatic repulsion among $Ca(RSO_4)^+$ complexes and the positively charged surface. Such charge reversal was also predicted by molecular dynamics simulations of silica with the presence of Ca^{2+} ions.[59,60]

On the basis of the experimental data obtained and the interpretation according to the Voigt model, we come to the following overall picture of AAS adsorption to clay surfaces (Figure 4d,e). Calcium ion is always needed for AAS adsorption to clay surfaces at pH = 9 and at room temperature. These Ca^{2+} ions act as a bridge between the negatively charged sites on the clay surface and the anionic head group of AAS. Already at low Ca^{2+} concentrations, AAS adsorption starts and the amount adsorbed increases with the Ca^{2+} concentration up to 200 mM. Desorption of AAS is fast if the flowing solution does not contain added AAS. Most likely, a multilayer of low density packed AAS is formed. The more Ca^{2+} present, the more bridges are formed (Figure 4d). On basis of polarity considerations, it is likely that the outer face of the AAS multilayer is hydrophilic. At still higher Ca^{2+} concentration (>200 mM), maximum AAS adsorption is reached, and the multilayer destabilizes at still higher Ca^{2+} concentrations, as was concluded from the observed lower frequency shift. It is suggested that the presence of such high Ca^{2+} concentrations leads to stabilization of the remaining multilayer. This is based on the low rate of AAS desorption under these conditions.

3.5. Mixed Cation Solutions.

So far, the effect of Na^+ and Ca^{2+} ions have been investigated in separate experiments. In the presence of Na^+, no AAS adsorption promoting effect was observed, whereas the presence of Ca^{2+} strongly favors AAS adsorption to the clay surfaces. Under the same conditions as before regarding AAS concentration, pH, and temperature, we have investigated the frequency shift (mass change) of our clay-modified QCM-D upon the application of mixed NaCl and $CaCl_2$ solutions, to investigate if there is any competing effect. The total added salt concentration was set to 100 mM. It is realized that for the same concentration of $CaCl_2$ compared to NaCl, we have in the former case the double amount of chloride ions present, the same amount of cations, however now of double charge. The results of the observed frequency shifts as a function of the fraction of $CaCl_2$ is shown in Figure 5a. If only 100 mM NaCl is present, the frequency shift is negligible (2 Hz) and no AAS adsorption occurs. Increasing the fraction of $CaCl_2$ shows a gradual increase of frequency shift, indicating that more mass (AAS) is adsorbed. This ends at a frequency shift of 28 Hz for only 100 mM $CaCl_2$. It is remarkable to see that in between these extreme fractions, the amount of adsorbed AAS decreases linearly with the decreasing fraction of $CaCl_2$. It can be explained by the decreasing cation bridging with the decrease of Ca^{2+} concentration. It was also found that the adsorption amount at 100 mM Ca^{2+} was twice than the adsorption at 50 mM Ca^{2+} and 50 mM Na^+ in mixed solutions. In Table 2, the adsorption in 100 mM Ca^{2+} was found to be larger than in only 50 mM Ca^{2+} but not twice the amount relationship. The plausible explanation is that Na^+ competes for the adsorption sites.

To further investigate the competitive adsorption behavior between Na^+ and Ca^{2+} in mixed solution, the adsorptions of AAS surfactant were performed at constant 50 mM Ca^{2+} with variable Na^+ concentrations (0, 10, 50, 100, 450 mM) and the results are shown in Figure 5b. From 0 to 50 mM Na^+, the surfactant adsorption was decreased with increasing Na^+ concentration, indicating that Na^+ indeed took some adsorption sites of Ca^{2+}. At 450 mM Na^+, a slight increase of adsorption was observed. The more Na^+ did not compete for more adsorption sites and the slightly increased adsorption came from the larger electric double layer force for strongly bound surfactants in higher salt concentrations. An estimation of the maximum competitive sites that Na^+ took is about 30%.

In our previous study on calcite surfaces,[26] surfactant adsorption remained stable and did not change at 50 mM Ca^{2+} when the Na^+ concentration was varied from 1 to 500 mM. However, for the silica surfaces, the adsorption decreased with increasing Na^+ concentration (1−500 mM) and with Ca^{2+} fixed at 50 mM. Based on the results on clay, calcite, and silica surfaces, we came to the conclusion that Na^+ is an indifferent ion on the calcite surface for the surfactant adsorption, but it could replace all the Ca^{2+} binding sites on the silica because the interaction between the Si−O anion with the Ca cation is weaker compared to the interaction between the carbonate anion and the Ca cation. It also suggests that there are at least two sites for Ca^{2+} binding on the clay surface, one is related to the present Al(III) sites and the other is surface silanol. The first type seems to lead to the stable Ca cation binding that is similar to the calcite surface. The other is the less stable Ca cation binding, similar to the silica surface. In this picture, the competing behavior between Na^+ and Ca^{2+} on clay surface is in between calcite and silica surfaces. The overall binding properties of a Ca^{2+} ion plus an AAS surfactant molecule to the binding site on clay is much stronger than the binding of only a Na^+ ion.

3.6. Salinity Effect.

The LS water flooding as a method for surfactant-free EOR has been proven effective, which releases more oil from sandstone reservoirs than conventional flooding with seawater or formation water.[21,29,30] The combined surfactant with LS injection for EOR reported a higher oil recovery compared to applying LS or surfactant flooding separately.[61] In this section, we describe our investigation of the effect of LS and HS conditions on the AAS adsorption to clay surfaces at pH = 9 and room temperature. The composition of the LS and HS solutions investigated is given in Table 3. The recipe for artificial seawater, which served as the HS solution, was similar to those reported previously.[21] For the LS and LS-no Ca solution, we simply diluted the stock HS and HS-no Ca solutions by ∼25 times.

Table 3. Composition of the HS and LS solutions

salt	HS	HS/no Ca	LS	LS/no Ca
$CaCl_2$ (mM)	50	0	2	0
NaCl (mM)	450	450	18	18
salinity (ppm)	31 800	26 300	1270	1050

The surfactant adsorption behaviors under HS and LS in the presence and absence of Ca^{2+} were studied, as shown in Figure 6. The largest AAS surfactant adsorption was obtained in the HS solution. The change from HS to LS gave rise to a sharply decreased adsorption. Based on a previous AFM study on the pore-scale mechanism for the LS effect,[21] it can be attributed to the combined electric double layer repulsion and cation bridging effect. In the HS-no Ca solution, the adsorption shows comparable adsorption as in LS. The HS solution has similar salinity to HS-no Ca solution, but the adsorption is obviously lower in HS-no Ca. From these comparisons, the decreased adsorption from HS to LS is due to the lower of Ca^{2+}, which leads to less cation bridging but not the decreased electric double layer repulsion effect. After the removal of Ca^{2+} of LS, the lowest adsorption is shown in LS-no Ca solution. This observation suggests that the reduction of surfactant adsorption mainly depends on the number of divalent cations such as Ca^{2+} in the solution. The lower adsorption of surfactants in LS than HS stems from the less Ca^{2+} in LS and the Ca^{2+} can always bind to a clay surface that makes some adsorptions. To reduce surfactant adsorption in HS solution, it is not necessary to reduce the salinity of solution but more important to remove the residual divalent Ca^{2+} ions in solution.

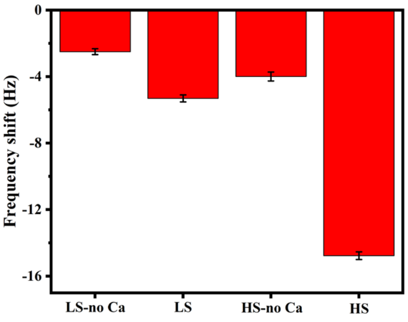

Figure 6. Effect of HS and LS solutions with and without Ca^{2+}on the AAS surfactant adsorption in the presence of 0.15 wt % AAS, at pH = 9.

3.7. Temperature Effect.

Finally, we have investigated the effect of increasing temperature (23−65 °C) on the frequency shift (mass change) of the clay-modified sensor of QCM-D upon addition of AAS (0.15 wt %) in 100 mM aqueous $CaCl_2$ at pH = 9. The results are presented in Figure 7. Increasing the temperature from 23 to 35 °C shows a small increase of frequency shift (more AAS adsorbed). Further increase of the temperature up to 65 °C shows a reduction of frequency shift (less AAS adsorbed) of about 20%. This is an interesting observation; first, a small increase in adsorbed AAS, followed by a decrease. In general, you expect for increasing the temperature that adsorption will be reduced. What could be the reason for increased adsorption in the range of 23−35 °C? This can be understood by realizing that the free AAS monomers are the adsorbing species. These AAS monomers are in equilibrium with monomers in the AAS micelles, and their concentration is equal to the cmc. As micelles are destabilized at higher temperatures, the cmc will increase at higher temperatures on the basis of our measurements, and therefore the AAS monomer concentration available for binding to the clay surface also increases. Clearly, in this temperature domain, the overall result is an increase of the amount of AAS adsorbed. At temperatures above 35 °C, the cmc will further rise from our study, resulting in more AAS monomers in the solution. At these temperatures, the

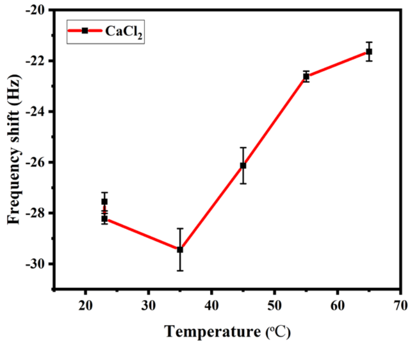

Figure 7. Frequency shift observed upon increasing the temperature from 23 to 65 °C in the presence of 0.15 wt % AAS, 100 mM $CaCl_2$, and at pH = 9.

adsorption of AAS to the clay surface will overall be reduced. Clearly, the reduced AAS adsorption at higher temperature is not compensated by the increase of AAS monomers. An increase in temperature leads to an increase in the kinetic energy of the species. The interaction between the surfactant and surface becomes weaker at higher temperatures. The relatively high kinetic energy and subsequent high entropy contribute to the decrease of aggregate organization of surfactant on the surface, giving rise to the low adsorption of surfactants. Similar adsorption behavior has been observed by Azam et al.,[24] who studied the adsorption of anionic surfactant onto crushed Berea sandstone. A shift to lower adsorption at high temperatures for sodium dodecyl sulfate on hydrotalcite-like minerals was also found.[62] This suggests the possibility of AAS surfactant used in high temperature with less adsorption, but should not too high because of its chemical stability.

3.8. Implications for Surfactant Adsorption. This study provided a relatively simple and fast way of screening experimental parameters of importance for surfactant adsorption to clay mineral surfaces, which can be used as an alternative to more time-consuming core flooding tests.[30] We have focused in this study on the role of clay species only, which do form part of sandstone and calcite rock formations. Calcium ions are always needed for anionic AAS surfactant adsorption on negatively charged surfaces. The extent of negative charge is determined by the rock composition (sandstone, calcite), the presence of clay species, and the pH of the solution. The more alkaline the solution, the more negative charge is present. The present Ca^{2+} ions act as a bridge between these negative surface sites and the negatively charged head group of the AAS surfactants. The more Ca^{2+}, the more AAS can be bound. This is true up to 200 mM Ca^{2+} at pH = 9. Higher Ca^{2+} concentrations destabilize the low-density multilayer and a thinner denser multilayer is proposed to be formed. The increased stability of the adsorbed layer could come from the increased electric double layer force and the strong screening effect of Ca^{2+}. However, the Na^+ could compete for adsorption sites in the Ca^{2+} and Na^+ mixed solutions and an estimation of the maximum competitive sites that Na^+ took was about 30% on the clay surface, which is in between silica and calcite surfaces. Increasing the temperature from 23 to 65 °C shows first a small increase of AAS adsorbed followed by a reduction of AAS adsorbed. The balance of interactions of AAS monomers in solution, in micelles, and bound to the clay surface determine the overall effect. To reduce the surfactant adsorption, one of the key issues is to control the divalent cations such as Ca^{2+} in solutions or improve the divalent cation tolerance of surfactants.

4. CONCLUSIONS

To gain insights into surfactant adsorption on mineral surfaces, QCM-D was exploited to study the adsorption behavior of anionic AAS surfactant to the clay surface under various cation conditions. The experimental results and consequent analysis revealed new fundamental features of adsorption behavior of surfactants. In the presence of Ca^{2+} ions, the AAS adsorption increased with increasing pH, whereas it decreased in the solution containing Na^+ solution. It is proposed that the sulfate anionic head group of AAS binds to the negatively charged clay surface via a bridging Ca^{2+} ion. For a fixed pH = 9, the surfactant adsorption goes through a maximum (~200 mM) at increasing Ca^{2+} concentrations. The experimental data of frequency shift and dissipation shift have been analyzed using three different models, in which the Voigt model better described the multilayer adsorption, as many as 4−6 monolayers in 200 mM $CaCl_2$ solution. For the experiments with varying NaCl concentrations, it is seen that there is hardly any AAS adsorption, over the entire investigated concentration range.

In a mixed cation (Ca^{2+} and Na^+) solution, the amount of adsorbed AAS decreased linearly with decreasing fraction of $CaCl_2$. However, Na^+ competed for some adsorption sites and an estimation of the maximum competitive sites that Na^+ took was about 30%. The significant role of Ca^{2+} for the adsorption of AAS to the clay surface was stressed when HS was switched to LS solutions. The reduction of surfactant adsorption from HS to LS mainly depended on the decreased amount of Ca^{2+} and the electric double layer effect was of minor importance. Furthermore, increasing the temperature from 23 to 65 °C shows first a small increase of AAS adsorbed followed by a reduction of AAS adsorbed. The new fundamental understanding about cation-dependent surfactant adsorption contributes to optimizing the injection conditions of surfactants, which is useful to develop more effective EOR approaches and it could also be applied over a range of disciplines, including improved remediation strategies for contaminated soil and groundwater.

■ ASSOCIATED CONTENT

Ⓢ Supporting Information

The Supporting Information is available free of charge at https://pubs.acs.org/doi/10.1021/acs.energyfuels.9b03109.

> High magnification SEM images of clay surface on the same area (a) ×1000 magnified and (b) ×10 000 magnified; XPS measurable area is in the center of sputtering area on the clay surface;survey scan after sputtering; and XPS results of clay surface with binding energy positions, full width at half-maximum, and relative percentages of each element (PDF)

■ AUTHOR INFORMATION

Corresponding Authors

*E-mail: zlliu89@gmail.com (Z.L.).
*E-mail: E.J.R.Sudholter@tudelft.nl (E.J.R.S.).

ORCID

Zilong Liu: 0000-0003-1023-177X
Ernst J. R. Sudhölter: 0000-0003-3296-953X

Notes

The authors declare no competing financial interest.

■ ACKNOWLEDGMENTS

The authors thank Dr. M. Brewer and Dr. J. van Wunnik (Shell Global Solutions) for providing surfactant samples and for their active discussions. Technical assistance from Duco Bosma and Bart Boshuizen of TuD is appreciated. Financial support was provided by Shell Global Solutions.

■ REFERENCES

(1) Lin, S. H.; Leu, H. G. Operating Characteristics and Kinetic Studies of Surfactant Wastewater Treatment by Fenton Oxidation. *Water Res.* **1999**, *33*, 1735−1741.

(2) Sabah, E.; Turan, M.; Celik, M. S. Adsorption mechanism of cationic surfactants onto acid- and heat-activated sepiolites. *Water Res.* **2002**, *36*, 3957−3964.

(3) Li, C.; Dong, Y.; Wu, D.; Peng, L.; Kong, H. Surfactant Modified Zeolite as Adsorbent for Removal of Humic Acid from Water. *Appl. Clay Sci.* **2011**, *52*, 353−357.

(4) Qu, J.; Tao, X.; He, H.; Zhang, X.; Xu, N.; Zhang, B. Synergistic Effect of Surfactants and a Collector on the Flotation of a Low-Rank Coal. *Int. J. Coal Prep. Util.* **2015**, *35*, 14−24.

(5) Hirasaki, G.; Miller, C. A.; Puerto, M. Recent Advances in Surfactant EOR. *SPE J.*, 2011; Vol. *16* (04), pp 889−907.

(6) Lake, L. W.; Johns, R. T.; Rossen, W. R.; Pope, G. A. *Fundamentals of Enhanced Oil Recovery*, 2014, Society of Petroleum Engineers.

(7) Tagavifar, M.; Jang, S. H.; Sharma, H.; Wang, D.; Chang, L. Y.; Mohanty, K.; Pope, G. A. Effect of PH on Adsorption of Anionic Surfactants on Limestone: Experimental Study and Surface Complexation Modeling. *Colloids Surf. Physicochem. Eng. Asp.* **2018**, *538*, 549−558.

(8) Elias, S. D.; Rabiu, A. M.; Oluwaseun, O.; Seima, B. Adsorption Characteristics of Surfactants on Different Petroleum Reservoir Materials. *Online J. Sci. Technol.*, **2016**, *6*, 6−16.

(9) Ahmadi, M. A.; Shadizadeh, S. R. Experimental Investigation of a Natural Surfactant Adsorption on Shale-Sandstone Reservoir Rocks: Static and Dynamic Conditions. *Fuel* **2015**, *159*, 15−26.

(10) Durán-Álvarez, A.; Maldonado-Domínguez, M.; González-Antonio, O.; Durán-Valencia, C.; Romero-Avila, M.; Barragán-Aroche, F.; López-Ramírez, S. Experimental−Theoretical Approach to the Adsorption Mechanisms for Anionic, Cationic, and Zwitterionic Surfactants at the Calcite−Water Interface. *Langmuir* **2016**, *32*, 2608−2616.

(11) Park, S.; Lee, E. S.; Sulaiman, W. R. W. Adsorption Behaviors of Surfactants for Chemical Flooding in Enhanced Oil Recovery. *J. Ind. Eng. Chem.* **2015**, *21*, 1239−1245.

(12) Al Mahrouqi, D.; Vinogradov, J.; Jackson, M. D. Zeta Potential of Artificial and Natural Calcite in Aqueous Solution. *Adv. Colloid Interface Sci.* **2017**, *240*, 60−76.

(13) Zhang, R.; Somasundaran, P. Advances in adsorption of surfactants and their mixtures at solid/solution interfaces. *Adv. Colloid Interface Sci.* **2006**, *123−126*, 213−229.

(14) Mahani, H.; Menezes, R.; Berg, S.; Fadili, A.; Nasralla, R.; Voskov, D.; Joekar-Niasar, V. Insights into the Impact of Temperature on the Wettability Alteration by Low Salinity in Carbonate Rocks. *Energy Fuels* **2017**, *31*, 7839−7853.

(15) Saxena, N.; Kumar, A.; Mandal, A. Adsorption Analysis of Natural Anionic Surfactant for Enhanced Oil Recovery: The Role of Mineralogy, Salinity, Alkalinity and Nanoparticles. *J. Pet. Sci. Eng.* **2019**, *173*, 1264−1283.

(16) Al-Khafaji, A.; Neville, A.; Wilson, M.; Wen, D. Effect of Low Salinity on the Oil Desorption Efficiency from Calcite and Silica Surfaces. *Energy Fuels* **2017**, *31*, 11892−11901.

(17) Kamal, M. S.; Hussein, I. A.; Sultan, A. S. Review on Surfactant Flooding: Phase Behavior, Retention, IFT, and Field Applications. *Energy Fuels* **2017**, *31*, 7701−7720.

(18) Wesson, L. L.; Harwell, J. H. Surfactant Adsorption in Porous Media. *Surfactants Fundamentals and Applications in the Petroleum Industry*; Cambridge University Press, 2000; pp 121−158.

(19) Pillai, P.; Mandal, A. Wettability Modification and Adsorption Characteristics of Imidazole-Based Ionic Liquid on Carbonate Rock: Implications for Enhanced Oil Recovery. *Energy Fuels* **2019**, *33*, 727−738.

(20) Solairaj, S.; Britton, C.; Kim, D. H.; Weerasooriya, U.; Pope, G. A. Measurement and Analysis of Surfactant Retention. In *SPE Improved Oil Recovery Symposium*; Society of Petroleum Engineers, 2012.

(21) Liu, Z. L.; Rios-Carvajal, T.; Andersson, M. P.; Ceccato, M.; Stipp, S. L. S.; Hassenkam, T. Insights into the Pore-Scale Mechanism for the Low-Salinity Effect: Implications for Enhanced Oil Recovery. *Energy Fuels* **2018**, *32*, 12081−12090.

(22) Hirasaki, G.; Zhang, D. L. Surface Chemistry of Oil Recovery from Fractured, Oil-Wet, Carbonate Formations. *Spe J.* **2004**, *9*, 151−162.

(23) AlQuraishi, A. A.; AlHussinan, S. N.; AlYami, H. Q. Efficiency and Recovery Mechanisms of Low Salinity Water Flooding in Sandstone and Carbonate Reservoirs. In *Offshore Mediterranean Conference and Exhibition*, 2015.

(24) Azam, M. R.; Tan, I. M.; Ismail, L.; Mushtaq, M.; Nadeem, M.; Sagir, M. Static adsorption of anionic surfactant onto crushed Berea sandstone. *J. Pet. Explor. Prod. Technol.* **2013**, *3*, 195−201.

(25) Salari, Z.; Ahmadi, M. A. Experimental studies of ionic surfactant adsorption onto carbonate rocks. *Environ. Eff.* **2016**, *38*, 549−554.

(26) Haaring, R.; Kumar, N.; Bosma, D.; Poltorak, L.; Sudholter, E. J. Electrochemically-Assisted Deposition of Calcite for Application in Surfactant Adsorption Studies. *Energy Fuels* **2019**, *33*, 805.

(27) Wanless, E. J.; Ducker, W. A. Weak Influence of Divalent Ions on Anionic Surfactant Surface-Aggregation. *Langmuir* **1997**, *13*, 1463−1474.

(28) Wang, F. H. L. Effects of Reservoir Anaerobic, Reducing Conditions on Surfactant Retention in Chemical Flooding. *SPE Reserv. Eng.* **1993**, *8*, 108−116.

(29) Tang, G.-Q.; Morrow, N. R. Influence of Brine Composition and Fines Migration on Crude Oil/Brine/Rock Interactions and Oil Recovery. *J. Pet. Sci. Eng.* **1999**, *24*, 99−111.

(30) Lager, A.; Webb, K. J.; Black, C. J. J. Impact of Brine Chemistry on Oil Recovery. In *IOR 2007-14th European Symposium on Improved Oil Recovery*, 2007.

(31) Kalwar, S. A.; Elraies, K. A.; Memon, M. K.; Kumar, S.; Abbas, G.; Mithani, A. H. A New Approach to ASP Flooding in High Saline and Hard Carbonate Reservoirs. In *International Petroleum Technology Conference*, 2014.

(32) Ma, K.; Cui, L.; Dong, Y.; Wang, T.; Da, C.; Hirasaki, G. J.; Biswal, S. L. Adsorption of Cationic and Anionic Surfactants on Natural and Synthetic Carbonate Materials. *J. Colloid Interface Sci.* **2013**, *408*, 164−172.

(33) Sánchez-Martín, M. J.; Dorado, M. C.; Del Hoyo, C.; Rodríguez-Cruz, M. S. Influence of Clay Mineral Structure and Surfactant Nature on the Adsorption Capacity of Surfactants by Clays. *J. Hazard. Mater.* **2008**, *150*, 115−123.

(34) Amirianshoja, T.; Junin, R.; Kamal Idris, A.; Rahmani, O. A Comparative Study of Surfactant Adsorption by Clay Minerals. *J. Pet. Sci. Eng.* **2013**, *101*, 21−27.

(35) Torn, L. H.; De Keizer, A.; Koopal, L. K.; Lyklema, J. Mixed adsorption of poly(vinylpyrrolidone) and sodium dodecylbenzenesulfonate on kaolinite. *J. Colloid Interface Sci.* **2003**, *260*, 1−8.

(36) Rodríguez-Cruz, M. S.; Sanchez-Martin, M. J.; Sanchez-Camazano, M. A Comparative Study of Adsorption of an Anionic and a Non-Ionic Surfactant by Soils Based on Physicochemical and Mineralogical Properties of Soils. *Chemosphere* **2005**, *61*, 56−64.

(37) Suzzoni, A.; Barre, L.; Kohler, E.; Levitz, P.; Michot, L. J.; M'Hamdi, J. Interactions between Kaolinite Clay and AOT. *Colloids Surf. Physicochem. Eng. Asp.* **2018**, *556*, 309−315.

(38) Figdore, P. E. Adsorption of Surfactants on Kaolinite: NaCl versus CaCl2 Salt Effects. *J. Colloid Interface Sci.* **1982**, *87*, 500−517.

(39) Wang, L.; Siretanu, I.; Duits, M. H. G.; Stuart, M. A. C.; Mugele, F. Ion Effects in the Adsorption of Carboxylate on Oxide Surfaces, Studied with Quartz Crystal Microbalance. *Colloids Surf. Physicochem. Eng. Asp.* **2016**, *494*, 30−38.

(40) Adkins, S.; Liyanage, P. J.; Arachchilage, P.; Gayani, W. P.; Mudiyanselage, T.; Weerasooriya, U.; Pope, G. A. A New Process for Manufacturing and Stabilizing High-Performance EOR Surfactants at Low Cost for High-Temperature, High-Salinity Oil Reservoirs. In *SPE Improved Oil Recovery Symposium*; Society of Petroleum Engineers, 2010.

(41) Guo, Y.; Yu, X. Characterizing the Surface Charge of Clay Minerals with Atomic Force Microscope (AFM). *AIMS Mater. Sci.* **2017**, *4*, 582−593.

(42) Liu, Z.; Nørgaard, K.; Overgaard, M. H.; Ceccato, M.; Mackenzie, D. M. A.; Stenger, N.; Stipp, S. L. S.; Hassenkam, T. Direct Observation of Oxygen Configuration on Individual Graphene Oxide Sheets. *Carbon* **2018**, *127*, 141−148.

(43) Moulder, J. F. *Handbook of X-Ray Photoelectron Spectroscopy*; Perkin-Elmer Corporation, 1995; pp 230−232.

(44) Sauerbrey, G. n. Verwendung von Schwingquarzen Zur Wägung Dünner Schichten Und Zur Mikrowägung. *Z. Für Phys.* **1959**, *155*, 206−222.

(45) Rodahl, M.; Höök, F.; Krozer, A.; Brzezinski, P.; Kasemo, B. Quartz crystal microbalance setup for frequency and Q-factor measurements in gaseous and liquid environments. *Rev. Sci. Instrum.* **1995**, *66*, 3924−3930.

(46) Voinova, M. V.; Rodahl, M.; Jonson, M.; Kasemo, B. Viscoelastic Acoustic Response of Layered Polymer Films at Fluid-Solid Interfaces: Continuum Mechanics Approach. *Phys. Scr.* **1999**, *59*, 391.

(47) Hu, X.; Yutkin, M. P.; Hassan, S.; Wu, J.; Prausnitz, J. M.; Radke, C. J. Calcium Ion Bridging of Aqueous Carboxylates onto Silica: Implications for Low-Salinity Waterflooding. *Energy Fuels* **2018**, *33*, 127−134.

(48) Hassenkam, T.; Pedersen, C. S.; Dalby, K.; Austad, T.; Stipp, S. L. S. Pore Scale Observation of Low Salinity Effects on Outcrop and Oil Reservoir Sandstone. *Colloids Surf. Physicochem. Eng. Asp.* **2011**, *390*, 179−188.

(49) Sposito, G.; Skipper, N. T.; Sutton, R.; Park, S.-h.; Soper, A. K.; Greathouse, J. A. Surface Geochemistry of the Clay Minerals. *Proc. Natl. Acad. Sci.* **1999**, *96*, 3358−3364.

(50) Sondi, I.; Biščan, J.; Pravdić, V. Electrokinetics of Pure Clay Minerals Revisited. *J. Colloid Interface Sci.* **1996**, *178*, 514−522.

(51) Pecini, E. M.; Avena, M. J. Measuring the Isoelectric Point of the Edges of Clay Mineral Particles: The Case of Montmorillonite. *Langmuir* **2013**, *29*, 14926−14934.

(52) Franks, G. V.; Gan, Y. Charging Behavior at the Alumina-Water Interface and Implications for Ceramic Processing. *J. Am. Ceram. Soc.* **2007**, *90*, 3373−3388.

(53) Bera, A.; Kumar, T.; Ojha, K.; Mandal, A. Adsorption of Surfactants on Sand Surface in Enhanced Oil Recovery: Isotherms, Kinetics and Thermodynamic Studies. *Appl. Surf. Sci.* **2013**, *284*, 87−99.

(54) Liu, Z.; Rios-Carvajal, T.; Andersson, M. P.; Stipp, S.; Hassenkam, T. Ion Effects on Molecular Interaction between Graphene Oxide and Organic Molecules. *Environ. Sci. Nano* **2019**, *6*, 2281.

(55) Abudu, A.; Goual, L. Adsorption of Crude Oil on Surfaces Using Quartz Crystal Microbalance with Dissipation (QCM-D) under Flow Conditions. *Energy Fuels* **2009**, *23*, 1237−1248.

(56) Collins, J.; Funfschilling, D.; Dennin, M. Langmuir Blodgett Films of Arachidic Acid and a Nematic Liquid Crystal: Characterization and Use in Homeotropic Alignment. *Thin Solid Films* **2006**, *496*, 601−605.

(57) Kele, P.; Orbulescu, J.; Mello, S. V.; Mabrouki, M.; Leblanc, R. M. Langmuir and Langmuir−Blodgett Film Characterization of a New Amphiphilic Coumarin Derivative. *Langmuir* **2001**, *17*, 7286−7290.

(58) Griffin, L. R.; Browning, K. L.; Lee, S. Y.; Skoda, M. W. A.; Rogers, S.; Clarke, S. M. Multilayering of Calcium Aerosol-OT at the Mica/Water Interface Studied with Neutron Reflection: Formation of a Condensed Lamellar Phase at the CMC. *Langmuir* **2016**, *32*, 13054−13064.

(59) Lorenz, C. D.; Travesset, A. Charge Inversion of Divalent Ionic Solutions in Silica Channels. *Phys. Rev. E* **2007**, *75*, 061202.

(60) Turesson, M.; Labbez, C.; Nonat, A. Calcium Mediated Polyelectrolyte Adsorption on Like-Charged Surfaces. *Langmuir* **2011**, *27*, 13572−13581.

(61) Johannessen, A. M.; Spildo, K. Enhanced Oil Recovery (EOR) by Combining Surfactant with Low Salinity Injection. *Energy Fuels* **2013**, *27*, 5738−5749.

(62) Pavan, P. C.; Crepaldi, E. L.; Gomes, G. d. A.; Valim, J. B. Adsorption of Sodium Dodecylsulfate on a Hydrotalcite-like Compound. Effect of Temperature, PH and Ionic Strength. *Colloids Surf. Physicochem. Eng. Asp.* **1999**, *154*, 399−410.